Sensors & Actuators: B. Chemical 436 (2025) 137640

Contents lists available at ScienceDirect

Sensors and Actuators: B. Chemical

journal homepage: www.elsevier.com/locate/snb

Glucose selective textile OECT based on molecularly imprinted nanoparticles functionalized channel for *in vivo* plants monitoring

Filippo Vurro [a], Elena Dembech [a], Riccardo Manfredi [a], Gabriele Debbi [a], Manuele Bettelli [a], Alice Marinangeli [b], Alessandra Maria Bossi [b], Nadia Palermo [a], Vittoria Martini [a], Michela Janni [a], Nicola Coppedè [a,*]

[a] IMEM-CNR Institute of Materials for Electronics and Magnetism, Italian National Research Council, Parco Area delle Scienze, 37/A, Parma 43124, Italy
[b] University of Verona, Department of Biotechnology, Strada Le Grazie 15, Verona 37134, Italy

ARTICLE INFO

Keywords:
Molecularly imprinted polymers (MIP)
Organic electrochemical transistor (OECT)
D-glucose detection
in vivo plant monitoring
Drought
Bioristor

ABSTRACT

Organic electrochemical transistors (OECTs) have been used as flexible biosensors, in organic bioelectronics, with high sensitivity and high transconductance but limited selectivity. OECTs can measure metabolic biomarkers, also continuously with real-time monitoring applications, in different biofluids of interest, with applications in sports, healthcare, biology and agriculture. In this study we developed an OECTs biosensor based on the functionalization of the active channel of the OECT with a biomimetic recognition element, namely molecularly imprinted nanoparticles (nanoMIPs), to selectively bind the target analyte D-glucose. Two configurations based on textile absorbent materials (nanoMIP fiber wire) or on polymer microfibers (nanoMIP microwire) were prepared and tested for D-glucose sensing and for D-fructose interference. The results show that the nanoMIPs improved the sensitivity and selectivity towards D-glucose. The nanoMIP fiber D-glucose wire sensor was used to monitor tomato plants in the field together with the conventional OECT based biosensor bioristor, providing new insights into the dynamics of the drought defense response.

1. Introduction

Organic electrochemical transistors (OECTs) serve as versatile biosensors in various bioelectronic applications due to their unique properties [1]. Specifically, OECTs are devices that utilize ionic currents for signal amplification and conductivity modulation through electrochemical doping processes [1]. The conductive polymer poly(3, 4-ethylene-dioxythiophene) doped with poly(styrene sulfonate) (PEDOT:PSS) has been extensively used in OECT applications due to its unique properties, such as transparency and flexibility, biocompatibility, and high electrical conductivity [2]. OECTs excel in transducing changes in ionic signals in a fluid environment into significant variations in electronic output signals, providing the requisite high sensitivity [3] for detecting subtle biological signals. Their fast response time, attributed to high transconductance [4], makes them suitable for measuring changes in biological signals.

OECTs offer easy miniaturization and integration with microfluidics [5,6], providing up to lab-on-a-chip devices for the detection of multiple analytes on a single platform [7,8]. Operating at low voltages and with minimal power consumption [3,7], OECTs are ideal for portable and implantable biosensing applications. Notably, they can be rendered biocompatible [9,10] by utilizing active materials and conductive polymers, aligning with biological systems. In particular, OECTs are intended for the conversion of biological signals from body fluids into electrical signals; thus, applications of OECTs are particularly directed at the monitoring of target molecules in biofluids, such as lactate [11], glucose [12], urea [13], salts [14,15], while more recently have been found in the early detection of cancer [16]. Additionally, OECT biosensors have also been developed for food safety to detect pathogens such as *E. coli* [17] and *Salmonella spp.* [18], as well as toxins to prevent bacterial contamination [19,20].

Moreover, thanks to their biocompatibility, flexibility, and stability, OECTs have been developed and implemented *in vivo* in living plants [21]. This sensor, namely the Bioristor [21], can detect the changes in

* Corresponding author.
E-mail addresses: filippo.vurro@imem.cnr.it (F. Vurro), elena.dembech@imem.cnr.it (E. Dembech), riccardo.manfredi@cnr.it (R. Manfredi), gabriele.debbi@imem.cnr.it (G. Debbi), manuele.bettelli@cnr.it (M. Bettelli), alice.marinangeli@univr.it (A. Marinangeli), alessandramaria.bossi@univr.it (A.M. Bossi), nadia.palermo@imem.cnr.it (N. Palermo), vittoria.martini@unipr.it (V. Martini), michela.janni@cnr.it (M. Janni), nicola.coppede@cnr.it (N. Coppedè).

https://doi.org/10.1016/j.snb.2025.137640
Received 26 November 2024; Received in revised form 10 March 2025; Accepted 16 March 2025
Available online 20 March 2025

the composition of the plant sap in growing plants, *in vivo* and in real-time, without interfering with their phyiological functions [22–24]. Bioristor enables the measurement of ion concentrations and movements in the vascular tissues of the plant, with a focus on the xylem vessels, which are responsible for water and mineral nutrients (xylem sap) transport from roots to leaves through the transpiration stream [9, 22]. Through the bioristor, novel information was acquired on the *in vivo* detection and monitoring of plant physiological mechanisms related to ion movement and compartmentalization, under both normal and stress conditions such as drought [22] and salt stress [23], or under environmental variations such as vapor pressure deficit (VPD) and increments in relative air relative humidity (RH) [25,26].

Critical to the OECT performance is the ability to selectively recognize specific targets. This is usually achieved by molecular recognition elements, such as antibodies [27–29], enzymes [30], or aptamers [31, 32]. However, these biological recognition elements have limitations, prompting a novel approach in the field: the use of biomimetic recognition elements and, specifically, of molecularly imprinted polymeric (MIP) materials.

MIPs are a distinctive class of polymeric biomimetics, prepared utilizing a template-assisted synthesis, in a process in which the polymer matrix is formed in the presence of a target analyte [33,34], this latter acting as a template. As a result, the synthetic materials obtained present molecular cavities that are complementary in shape, size, and stereochemistry to the target molecule of interest [35]. Recently, MIPs have also been synthesized in the form of nanoparticles, with resulting dimensions ranging from approximately 10 to 300 nm depending on the polymeric composition and on the synthetic approach, being this latter either a high-dilution approaches [36,37] or a solid-phase synthesis [38]. These nanometric MIPs are generally referred to as nanoMIPs.

In contrast to MIP membranes or to MIP bulk polymers, nanoMIPs are discrete homogeneous recognition elements, with a close resemblance to antibodies; in fact they exhibit a low number of binding sites per nanoparticle [39], fast interaction kinetics, and high affinities (dissociation constants $K_D \leq 10^{-9}$ M), tuned selectivity, while sharing the robustness and shelf-lives of polymers. NanoMIPs have a huge potential as "plastic receptors" to be integrated into sensors [40] and their use has been demonstrated to enhance the sensor sensitivity, respect to the use of bulk MIPs [41]. Several MIP-based sensors have been reported in the field of OECT, but to date, no example based on nanoMIPs has been reported. MIPs are characterized by high selectivity and sensitivity [34], making them a promising alternative to traditional recognition elements in OECT biosensors, while offering the stability, robustness, cost-effectiveness, and resistance to environmental factors typical of polymeric materials. Additionally, MIPs can be customized offering the possibility to design OECT biosensors specifically for diverse analytical applications.

OECT sensors based on MIPs have also been reported. In particular, MIPs in the form of membranes have been placed between the channel and the liquid electrolyte to create a selective layer [42]. Despite the selectivity, the MIP membrane might constitute an obstacle to the interaction of the ionic species with the active material, thus reducing the sensitivity of the sensor, and the membrane maintains an insulating factor that results in reducing the access of the ions and shielding the modulation effect that enables the mechanism of detection [43].

As an improvement in the coupling of MIPs and OECTs, imprinted membranes were implemented on the gate electrode [44]; this resulted in the reduction of the gate potential on the solution and allowed the detection of the sole species attracted by the gate electrode, typically for transistors with *p-type* conductivity channels.

OECTs based on MIPs (MIP-OECT) have been exploited for various biological measurements, mostly in the detection and recognition of biochemical compounds present in biofluids, for instance, MIP-OECT sensors for the detection of amino acid enantiomers, such as L/D-tyrosine and L/D-tryptophan [45], and L/D-histidine [46], have been reported. These approaches were highly sensitive and selective against their targets, due to the specific recognition of the imprinted cavities, and to the oxidation of the two amino acids, which generated distinct electrochemical signals, even at very low concentrations of the analytes, i.e. in the range from 300 nM to 10 μM. The amplification of the signal carried on by the transistor demonstrated the effectiveness of MIPs as a recognition element.

The application of MIP-OECTs has even been extended to the detection of ascorbic acid [47], to the discrimination of ammonium and tetrabutylammonium ions [48], to the non-invasive sensing of cortisol in sweat [43], for adrenaline and uric acid detection [49] in artificial urine thus aiming to meet the demands of diagnostic applications. In addition, MIP-OECTs have been developed for the quantification of dopamine [50], a marker for several neurological disorders, such as Parkinson's disease [51] and ADHD [52].

The developed sensor paves the way for real-time monitoring of the defense response triggered by plants during drought. Drought impacts affect both physiological and biochemical aspects related to photosynthesis, respiration, translocation, ion uptake, sugar and nutrient metabolism, and phytohormone balance [53–56]. Among these, sugar signaling, metabolism, and transport are important mechanisms for survival in such dehydration-induced challenges.

Drought stress not only induces sugar accumulation but also facilitates the breakdown of storage sugars (i.e. starch) into soluble sugars (i.e. sucrose, glucose, fructose, etc.) leading to a decrease in the water potential of the cell, a smart strategy to capture the limited moisture present in the soil [57].

Here we implemented the nanoMIP-based OECTs (nanoMIP-OECT) for glucose detection in tomato plants in open field and compared the glucose-specific signal with the conventional non-specific bioristor for the entire growing season under different irrigation volumes.

2. Experimental material and methods

2.1. Materials

All materials were analytical grade and used as received. D-glucose, D-fructose, acrylamide, N,N' methylene bisacrylamide (BIS), 3-(Acrylamido)phenylboronic acid (APBA), tert-butylacrylamide (tBAM), N,N,N′,N′-Tetramethyl ethylenediamine (TEMED), ammonium persulfate (APS), dodecyl benzene sulfonic acid (DBSA) were from Sigma Merck (Darmstadt, Germany); ethanol absolute, sulfuric acid 98 % from VWR Chemicals, poly(3,4-ethylenedioxythiophene)-poly(styrenesulfonate) (PEDOT:PSS) from Clevios PH1000, StarckGmbH.

2.2. Synthesis of the nanoMIPs

The synthesis of D-glucose 1X nanoMIP (12.5 μM) was carried out with 0.2 % w/v of template (T) and with a ratio template *versus* monomer (T:M) ratio of 1:150 in a final volume of 15 mL. All the monomer stock solutions were 2 % (w/v) in Milli-Q water while stock APBA was 2 % (w/v) in ethanol. A volume of 75 μL of APBA, 61 μL of acrylamide, and 55 μL of tBAM were admixed to the template, 160 μL of D-glucose (stock 8 mM) for 30 min under mild stirring. 1310 μL of BIS was added. The nanoMIP vials were closed with rubber caps; N_2 was bubbled through the reaction mixture for 15 min. Following the addition of 5 μL APS 40 % v/v and 5 μL TEMED the polymerization was carried out at 20 °C for 20 h. The nanoMIPs were extensively dialyzed overnight against 3 liters of Milli-Q water using a dialysis tube with 10000 MWCO (Sigma Aldrich, Milan, Italy). The synthesis of D-glucose 10X nanoMIP (125 μM, 0.2 %T; T:M 1:150) was carried out similarly except for the addition of 10 times more D-glucose.

2.3. Isothermal titration calorimetry

A Nano ITC Standard Volume (TA Instruments, Texas) with a fixed gold cell was used for titrating the nanoMIP imprinted with glucose with

D-glucose or with D-fructose. NanoMIPs were suspended in Milli-Q water at 1 mg/mL and titrant (D-glucose or D-fructose) at 100 μM; each sample was degassed under vacuum for 15 min before use. The reference cell was filled with 220 μL degassed Milli-Q water. The sample cell was filled with 220 μL nanoMIP and stirred at 250 rpm. The titrant (either D-glucose or D-fructose) was loaded into the syringe. The ITC experiment was conducted at 25 °C and consisted of 15 injections of 4 μL every 300 sec. A blank experiment, aimed at estimating the heat of dilution of the titrant, was performed by titrating water with the D-glucose or with D-fructose respectively and the signal was then subtracted to that of the nanoMIP measure. Data were analyzed with the NanoAnalyze Data Analysis software v. 2.3.6 (TA Instruments, New Castle, DE), and the dissociation constant (K_D), the reaction stoichiometry (n), the enthalpy, entropy and free energy variation (ΔH, ΔS and ΔG) were calculated. Specifically, the affinity constant (K_a reciprocal of K_D) was estimated by fitting the binding isotherm obtained from the heat changes upon titration, with the following equation:

$$q_i = \frac{nV_0\Delta H K_a[M_0]\,(1-\alpha_i)}{1+K_a[M_0]\,(1-\alpha_i)}$$

Where q_i = heat released or absorbed in the i^{th} injection; n is the stoichiometry of the binding interaction (molar ratio of ligand to macromolecule); V_0 the cell volume; ΔH is enthalpy change per mole of binding; K_a is the association constant; $[M_0]$ is the initial concentration of titrant in the cell; α_i fraction of macromolecule bound after the i^{th} injection. This equation is fitted to the binding isotherm (heat change vs. molar ratio) to estimate K_a; ΔH and n through nonlinear regression analysis. For the single-site binding model, the fraction of bound nanoMIP follows the classical Langmuir isotherm model.

2.4. The nanoMIP-OECT devices and their configuration

OECTs consist of a conductive polymer in contact with an electrolyte and a gate electrode immersed in the electrolytic solution. One of the most commonly used polymers to realize an OECT is the p-type conductive poly(3,4-ethylenedioxytiophene) doped with poly(styrene sulfonated) (PEDOT:PSS). The gate channel is often made of a metal wire (for example silver or copper) or of a wire functionalized with PEDOT:PSS. The drain current is generated by applying a drain-source voltage (V_{ds}) across the channel terminals, which drives holes along the polymer backbone. When a positive voltage is applied to the gate (V_g), the electrolytes present in the aqueous solutions are forced towards the nanoMIP film, interacting with the nanoMIP sites and de-doping the PEDOT. This reduces the number of carriers available and, consequently, the source-drain current (I_{ds}) decreases. Two types of OECT devices were developed for the detection of D-glucose from aqueous solutions. The first one, hereafter referred to as “nanoMIP microwire”, presents a drain-source channel made of a single microwire of PEDOT:PSS functionalized with D-glucose nanoMIPs, while the gate is made of a single PEDOT:PSS unfunctionalized microwire (Fig. 2A). The microwire was linked to the copper wires using a conductive silver paste.

To realize the nanoMIP microwire sensor for D-glucose detection, the first step was the preparation of the gate electrode: an aqueous solution of PEDOT:PSS, previously modified with the addition of DBSA surfactant (5 %), was injected directly into a beaker containing sulfuric acid (98 %) with a syringe equipped with a 0.6 mm needle, forming a continuous film of polymer microwire. The microwire formed was washed with distilled water and dried at 60 °C for 15 min. For the realization of the drain-source channel, a solution of PEDOT:PSS, modified with the addition of DBSA (5 %) and D-glucose nanoMIP (8 % w/w) was injected directly into a beaker containing sulfuric acid (98 %) with a syringe equipped with a needle of 0.6 mm diameter, forming a continuous film of modified polymer microwire. The microwire was then baked at 60 °C for 15 min. The second type of sensor, hereafter referred to as “nanoMIP fiber wire”, was prepared differently from the nanoMIP microwire: the drain-source channel is made of a polypropylene fiber coated with PEDOT:PSS solution and functionalized with nanoMIP imprinted with D-glucose, while the gate is made of a polypropylene fiber coated with unfunctionalized PEDOT:PSS (Fig. 1A). The drain-source and gate wires were connected to the copper wires using silver paste. The two sensors differ in size and material (Fig. 1B-C); the nanoMIP fiber wire sensor was easier to handle and less fragile than the nanoMIP microwire sensor. Two types of polypropylene fibers were used to develop the nanoMIP wire sensor for D-glucose detection, one for the gate channel and the other one for the drain-source channel. To realize the gate electrode, a polypropylene thread was soaked in an aqueous solution of PEDOT:PSS and DBSA surfactant (5 %); after soaking, the thread was baked at 120 °C for 15 min. This procedure was repeated three times. The polypropylene wire was then treated with sulfuric acid (98 %) for 15 min and washed with deionized water. For the realization of the drain-source channel, a polypropylene filament was soaked for three cycles in an aqueous solution of PEDOT:PSS and DBSA (5 %) and D-glucose nanoMIP (8 % w/w). After each soaking cycle, the polypropylene fiber was baked at 60 °C for 15 min. The wire was then treated with sulfuric acid (98 %) and washed with deionized water after 15 min. After the modification with the PEDOT:PSS solutions, the diameter of the polypropylene thread does not change and retains its flexibility and physical strength. A detailed sketch of the nanoMIP microwire and nanoMIP fiber wire OECT architectures is reported (Fig. 1D). A third type of sensor, based on the same architecture described for the wire sensor, was fabricated using the same unfunctionalized PEDOT:PSS fiber for both the gate and the drain-source channels and was considered as a negative control. SEM imaging was performed with by scanning electron microscopy (SEM, FlexSEM 1000, Hitachi, Tokyo, Japan).

2.5. Electric measurements

All electrical measurements for both OECT types were performed using a two-channel source/measure precision instrument benchtop SMU unit Agilent B2902A controlled by a home-made LabView 2024 software.

The dependence of the drain current (I_{ds}) as a function of time measured at a constant voltage (V_{ds}= −0.1 V) by pulsing the gate voltage from 0 to 1 V at 0.2 V steps was investigated for both the nanoMIP fiber wire and nanoMIP microwire sensors using D-glucose (10^{-6} M, 10^{-5} M, 10^{-4} M, 10^{-3} M, 10^{-2} M and 10^{-1} M) as the target analyte and D-fructose (10^{-6} M, 10^{-5} M, 10^{-4} M, 10^{-3} M, 10^{-2} M and 10^{-1} M) as the interfering compound. To simplify the comparison between the I_{ds} current variations of the two sensors in the presence of D-glucose and D-fructose, we normalized the measured current values I_{ds} with respect to the initial values I_{ds0}.

The responses of the sensors (R), given by the expression (I_{ds} - I_{ds0})/I_{ds0} where I_{ds0} represented the current across the channel when $V_g = 0$, were measured and plotted either as a function of the gate voltages V_g or as a function of the analyte concentrations [C] to compare the nanoMIP microwire and the nanoMIP fiber wire sensors.

Transfer characteristic curve was performed by measuring I_{ds} currents at increasing positive V_g values (from 0 to 1 V) at a constant V_{ds}= −0.1 V; output curves were performed by measuring I_{ds} currents for negative V_{ds} values (from 0 to −0.6) at increasing V_g (from 0 to 1 V).

In addition, the transconductance (g_m) was calculated and plotted as the change in output voltage (V_g) versus the change in input current (I_{ds}) to characterize the sensitivity and linearity of the devices to D-glucose and D-fructose.

2.6. Tomato measurements

A reduced water availability condition was applied in the field (60 % irrigation of the ideal water conditions). Four plants were equipped with four non-selective bioristor and four nanoMIP fiber wire OECT for D-glucose detection.

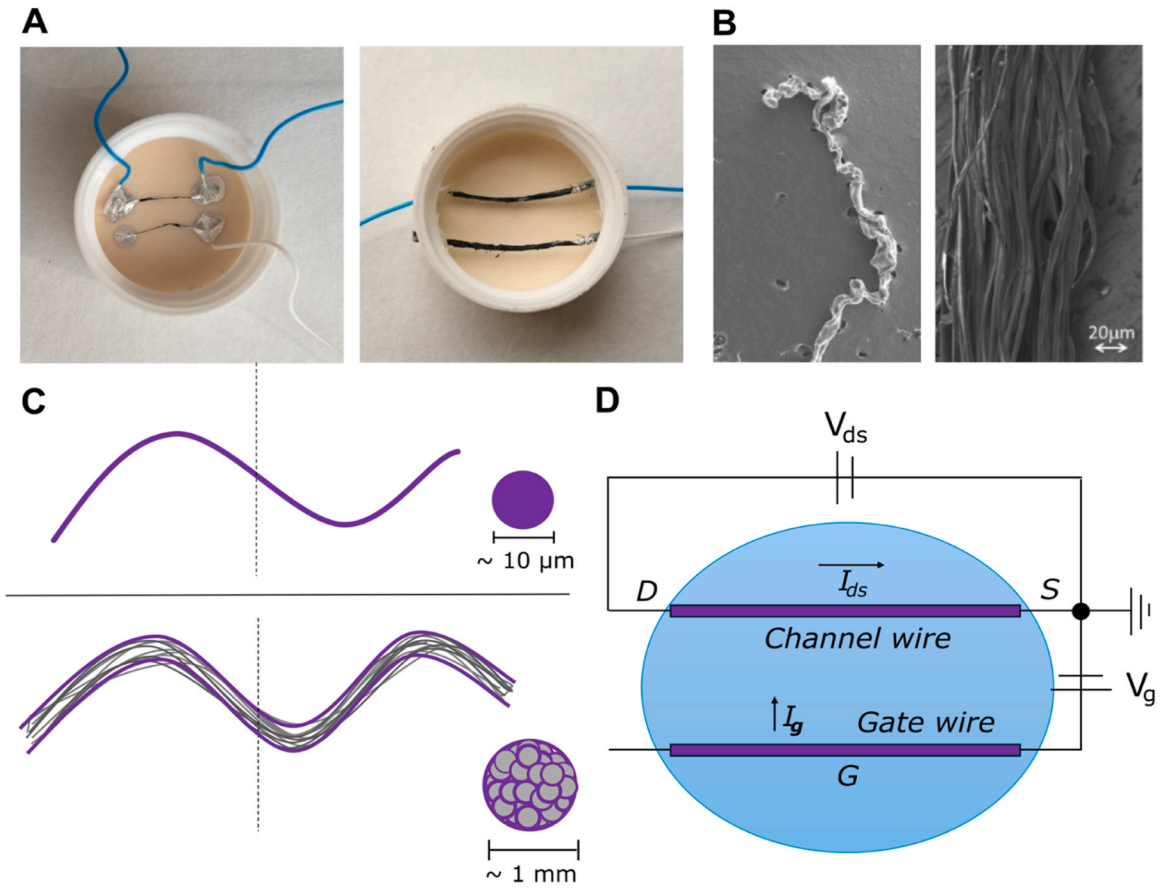

Fig. 1. NanoMIP OECT sensors. A) NanoMIP microwire (left) and nanoMIP fiber wire (right) OECT biosensors for glucose detection. B) SEM images of microwire and fiber wire before MIP functionalization. C) Schematic representation of the nanoMIP microwire (above) and the nanoMIP fiber wire (below) and their relative sections and dimensions. PEDOT:PSS layers are depicted in violet. D) Schematic of the OECTs composed of drain (D), source (S) and gate (S) electrodes immersed in the liquid sample.

The bioristor and the nanoMIP OECT were inserted into the plant stem of tomato plants with a distance of 5 mm between the two threads in tomato plants at 15 days after transplanting (5–6 leaves) at 10 cm above the soil surface [22–24] (Fig. 2A). The channel was connected by bonding two thin electric wires on both sides, while the gate is connected solely to the electrical wire on one side. These wires were fixed to a 3D-printed holder made of blue polymer material to improve the stability of the bioristor (Fig. 2A) and connected by wires to the digital motherboard (Fig. 2A) or the control unit (Fig. 2B).

A constant voltage (V_{ds} = −0.1 V) was applied between the source and drain terminals of the channel, resulting in a continuous current flow, and a positive voltage (V_g = 0.5 V) was applied to the gate, resulting in a decrease in channel conductivity due to cations being pushed into the channel from the electrolyte. The current (I_{ds}) was monitored continuously. The sensor response (R) was the main index obtained and was proportional cation concentration in the sap. It is given by the expression:

$$R = |I_{ds} - I_{ds0}| / I_{ds0} \quad (1)$$

where I_{ds0} represents the current across the channel when V_g = 0.

The sensor response R was recorded for the entire productive life cycle for the bioristor sensor. To acquire the value of the D-glucose

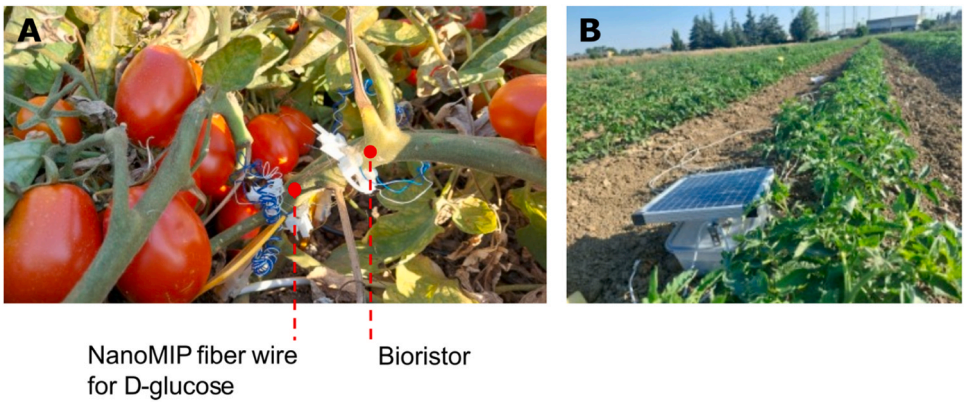

Fig. 2. Sensors implemented in tomato plants in field. A) NanoMIP fiber wire OECT for D-glucose detection and conventional bioristor, B) field control unit.

content, the nanoMIP fiber wire sensor response (gR) has been normalized with respect to the signal of the non-specific bioristor (R), prepared with the same geometrical structure but without MIP nanoparticles in the channel, obtaining a Normalized nanoMIP fiber wire value for D-glucose response (gNR=gR/R).

3. Result and discussion

3.1. D-glucose selective nanoMIPs

NanoMIPs were synthesized based on a monomer composition containing acrylamide derivatives, using BIS as a crosslinking agent (details in SI, Fig.S1), and choosing a one-pot synthesis strategy *via* free radical initiation in aqueous solution, as reported earlier [37]. D-glucose was used as a template for the imprinting process and was added to the monomer mixtures either 12.5 μM (1X) or 125 μM (10X). To favor the formation of D-glucose-specific binding sites, the functional monomer APBA was chosen, because it possesses the boronic acid group that enables it to form reversible covalent bonds with cis-diols. The choice was also supported by previous optimizations over the compositions of glucose-selective MIPs [58].

After the polymerization process, homogeneous colloidal nanomaterials were obtained as shown by dynamic light scattering (DLS), see Table 1. The hydrodynamic size of the nanoMIPs was further confirmed by scanning electron microscopy (SEM) images, as reported in SI (Fig. S2).

It was observed that the synthesized nanoMIPs were characterized by a small hydrodynamic size averaging around 20 nm. The polydispersity index (PDI) value varied between 0.3 and 0.4, indicating the formation of fairly homogeneous nanoparticulates. Additionally, at the completion of the synthesis, the imprinted nanoMIPs were subjected to extensive washing to remove the template and lyophilization for storage purposes. The lyophilised nanoMIPs were then resuspended and showed no significant changes in size or PDI with respect to the freshly synthesized ones, indicating the possibility of fully preserving the nanoMIPs (Table 1). Due to the higher homogeneity of the 10X nanoMIPs, compared to the 1X nanoMIPs, the 10X nanoMIPs were used for all the further experiments.

The imprinting of D-glucose on the nanoMIPs was confirmed by isothermal titration nanocalorimetry. A 1 mg/mL solution of nanoMIP was titrated with the template D-glucose (100 μM). During the titration, the binding events were measured as heat changes (μJ). The heat contribution specific for the nanoMIP/D-glucose binding event was quantified after the subtraction of the heat of dilution of D-glucose. The selectivity of nanoMIPs was assessed by monitoring the titration of nanoMIPs with D-fructose. The nanoMIP/D-fructose titration heat, subtracted from the heat of dilution, was compared with the nanoMIP/D-glucose (details in SI). It was reported that the thermodynamic parameters calculated by fitting the experimental data with the independent site model (details in SI, Fig.S3) showed a favorable enthalpic contribution ($\Delta H^\circ<0$) and an overall negative free energy change ($\Delta G^\circ<0$) was observed for the nanoMIP/D-glucose titrations, indicating spontaneous D-glucose binding under the experimental conditions. The affinity for D-glucose was estimated to be $K_D = 7.91 \pm 0.22 * 10^{-5}$ M with a number of binding sites per nanoparticle of about 27 ± 3, whereas in the case of D-fructose, the affinity was $K_D = 1.26 * 10^{-4}$ M and the estimated number of binding sites per nanoparticle was 33, suggesting that the interactions taking place were more labile for the non-template with respect to D-glucose. Overall, these results indicated the affinity of the nanoMIPs for their template, D-glucose, was about one order of magnitude higher than that observed for fructose, supporting the imprinting of D-glucose effectively occurred on the nanoMIPs. Concerning the number of binding sites, this appeared to be consistent for the binding of the template, D-glucose, and for fructose, suggesting the two sugars are bound by the same and finite number of sites, generated by the imprinting process. Given the great similarity in chemical functionalities and in size of the two sugars, a certain degree of recognition for fructose by the imprinted sites was expected. These results supported the ability of the 10X nanoMIPs to discriminate between D-glucose and fructose. The number of binding sites per nanoMIP (i.e. $n = 27 \pm 3$) correlates with the binding capacity of the nanoMIPs embedded in the sensor, hence it has an impact on the overall sensitivity of the sensor. The 10X nanoMIPs appeared as a suitable recognition element in the sensor, while further sensor's optimizations might imply to modify the molar ratio between D-glucose and the functional monomer so to modulate the number of binding sites per nanoMIP.

Table 1
physical parameters associated with D-glucose specific nanoMIPs.

Name	Hydrodynamic radius (nm)	Polydispersity Index
D-Glucose 10X nanoMIPs	18 ± 2	0.281 ± 0.023
D-Glucose 1X nanoMIPs	21 ± 2	0.430 ± 0.038
D-Glucose 10X nanoMIPs resuspended	22 ± 1	0.321 ± 0.028
D-Glucose 1X nanoMIPs resuspended	25 ± 4	0.410 ± 0.058

3.2. NanoMIP fiber wire and nanoMIP microwire OECT preparation

The two sensors, prepared as described in the experimental Section 2.4, consisted of a microwire based sensor with PEDOT:PSS and a nanoMIP channel, and a fiber wire-based sensor with PEDOT:PSS and a nanoMIP channel.

Potentiometric measurements were carried out in the presence of different concentrations of D-glucose (10^{-6} M, 10^{-5} M, 10^{-4} M, 10^{-3} M, 10^{-2} M and 10^{-1} M) as the target analyte and of D-fructose (10^{-6} M, 10^{-5} M, 10^{-4} M, 10^{-3} M, 10^{-2} M and 10^{-1} M) as the interfering compound to provide valuable information on the electrochemical properties of the nanoMIP-OECTs and their selectivity towards the D-glucose. These experiments were designed to demonstrate whether PEDOT:PSS based nanoMIP OECT devices were able to discriminate between D-glucose and an interfering compound and to verify its performance.

3.3. NanoMIP microwire characterization

D-glucose and D-fructose solutions in deionized water prepared at increasing concentrations were used to measure the I_{ds} current for the nanoMIP microwire as a function of time.

The I_{ds} current, measured by pulsing the gate voltage (V_g) between 0.2 V and 1.0 V with 0.2 V steps in the presence of D-glucose (Fig. 3A), had a negative slope for a positive V_g and reached a steady state with no further fluctuations in approximately 5 min. Measurements in deionized water, i.e. in the absence of the analyte, showed the I_{ds} ranging from −0.98 mA (at $V_g = 0.2$ V) to −0.94 mA (at $V_g = 0.8$ V). For increased concentrations of D-glucose, I_{ds} were reported from −0.98 mA (at $V_g = 0.2$ V) to −0.83 mA (at $V_g = 0.8$ V) when D-glucose was 10^{-6} M and from −0.98 mA (at $V_g = 0.2$ V) to −0.54 mA (at $V_g = 0.8$ V) for D-glucose at 10^{-1} M.

To assess the selectivity of the nanoMIP microwire, D-fructose was used as an interfering analyte, and the drain current I_{ds} was measured for increasing concentrations of D-fructose (Fig. 3B). It was observed that the I_{ds} of 10^{-1} M D-fructose decreased from −0.97 mA (at $V_g = 0.2$ V) to −0.88 mA (at $V_g = 0.8$ V).

The slopes of the I_{ds} measured for the D-fructose were significantly lower than those reported for D-glucose. The nanoMIP microwire device produced a lower response to interfering D-fructose molecules than D-glucose for all the concentrations tested, suggesting specific interactions taking place for the D-glucose with the nanoMIP layer.

The device response (R) was calculated as the ratio $(I_0\text{-}I)/I_0$, where "I" is the *off* current measured for gate voltages $V_g \neq 0$ and I_0 is the *on* current both measured for gate voltages $V_g = 0$. The responses of the

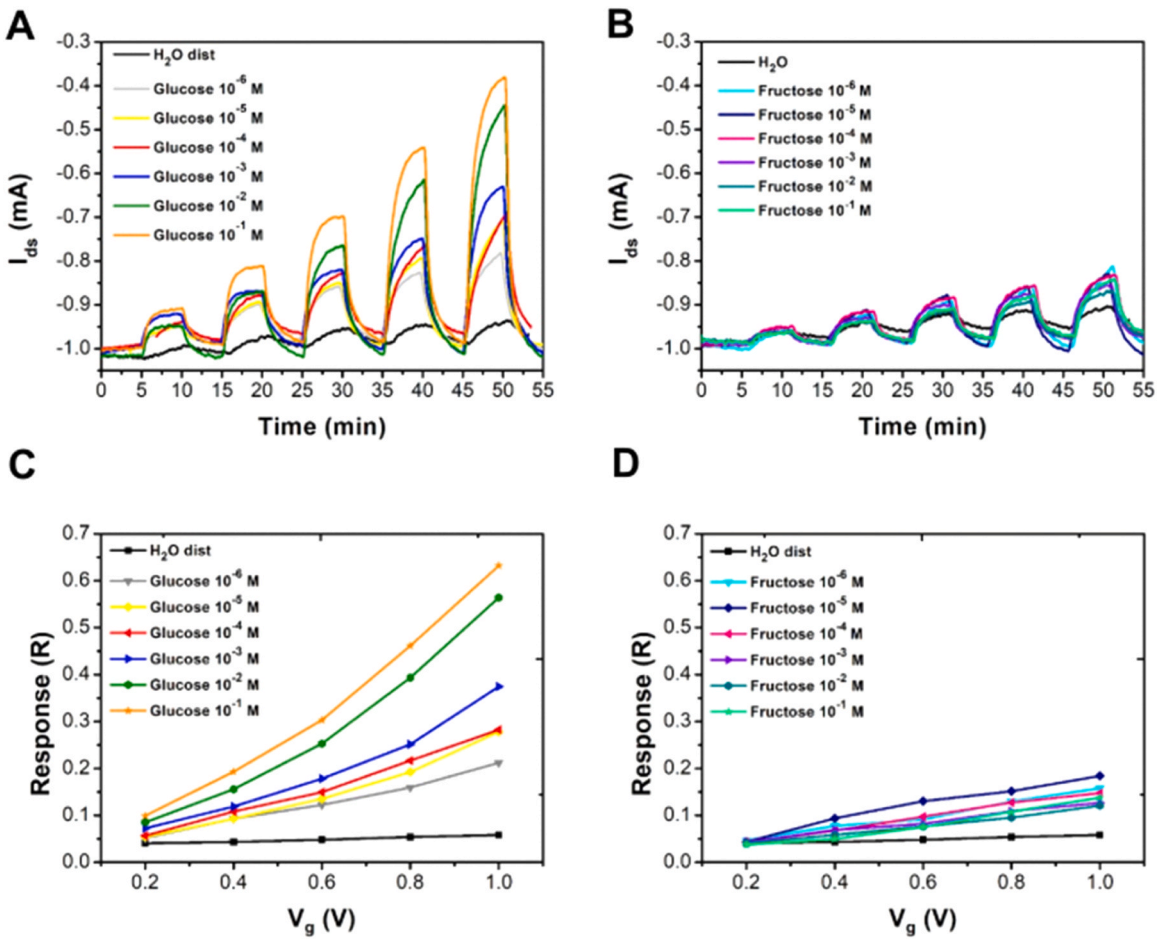

Fig. 3. NanoMIP microwire-based sensor properties. A) Drain current (I_{ds}) as a function of time in the presence of different D-glucose concentrations (10^{-6} M, 10^{-5} M, 10^{-4} M, 10^{-3} M, 10^{-2} M and 10^{-1} M) measured pulsing the gate voltage between 0.2 V and 1.0 V. B) Drain current (I_{ds}) as a function of time in the presence of different D-fructose concentrations (10^{-6} M, 10^{-5} M, 10^{-4} M, 10^{-3} M, 10^{-2} M and 10^{-1} M) measured pulsing the gate voltage between 0.2 V and 1.0 V. C) Calculated response (R) of the nanoMIP microwire sensor towards different D-glucose concentrations as a function of the applied gate voltage (V_g). D) Calculated response (R) of the nanoMIP microwire sensor towards different D-fructose concentrations as a function of the applied gate voltage (V_g).

nanoMIP microwire device for deionized water, D-glucose or D-fructose were analyzed.

Considering the sensor response for D-glucose, it was observed that it increased with increasing V_g for growing analyte concentrations. The highest response for D-glucose was equal to 0.46 and was observed for 10^{-1} M at $V_g = 0.8$ V. In contrast, the response to increasing concentrations of the interfering sugar was much lower than that calculated for the target analyte. The highest response for D-fructose was equal to 0.15 and was obtained for 10^{-5} M concentration (at $V_g = 0.8$ V), whereas the calculated R at 10^{-1} M D-fructose was 0.14 (at $V_g = 0.8$ V).

3.4. NanoMIP fiber wire characterization

Similar to the analysis performed on the nanoMIP microwire, the drain current I_{ds} of the textile fiber nanoMIP wire was measured by pulsing the gate voltage between 0.2 V and 1.0 V at 0.2 V steps in the presence of increasing D-glucose concentrations (Fig. 4A). The measurement was carried out using deionized water and D-glucose at different concentrations (10^{-4} M, 10^{-3} M, 10^{-2} M and 10^{-1} M) as the target analyte. The I_{ds} for the nanoMIP fiber wire sensor varied from −1.00 mA (at $V_g = 0.2$ V) to −0.92 mA (at $V_g = 0.8$ V) considering 10^{-1} M D-glucose.

In the case of increasing concentrations of D-fructose (10^{-4} M, 10^{-3} M, 10^{-2} M and 10^{-1} M), the I_{ds} of the glucose nanoMIP fiber wire sensor as a function of time showed less difference for the concentrations of the interfering compound (Fig. 4B) if compared to D-glucose. In fact, the drain current varied from −0.99 mA (at $V_g = 0.2$ V) to −0.96 mA (at Vg = 0.8 V) for D-fructose at 10^{-1} M concentration; when compared to the channel current measured for the nanoMIP microwire sensor, the decrease in drain current observed for the nanoMIP fiber wire sensor was noticeably lower.

The calculated response for the nanoMIP fiber wire sensor to D-glucose as a function of the applied V_g showed a similar trend to that characteristic of the nanoMIP microwire (Fig. 4C), with an improved response for the higher D-glucose concentration and for the maximum applied gate voltage.

In addition, the calculated response for the nanoMIP fiber wire sensor toward D-fructose as a function of the applied V_g suggested that the response of the sensor decreased with increasing concentration of D-fructose at $V_g = 0.8$ V, the response for 10^{-4} M D-fructose was 0.033 and for 10^{-1} M D-fructose was 0.025.

In the case of the nanoMIP fiber wire sensor, the calculated response for the target analyte was an order of magnitude lower than the response obtained for the nanoMIP microwire sensor, although the trend of the plotted R is the same for both sensors. We can hypothesize that the characteristic trend of the nanoMIP microwire sensor (Fig. 3C-D) depends on the higher volume/surface ratio of the nanoMIP microwire sensor if compared to the nanoMIP fiber wire sensor (Fig. 4C-D) resulting in a higher availability of the nanoMIP active sites.

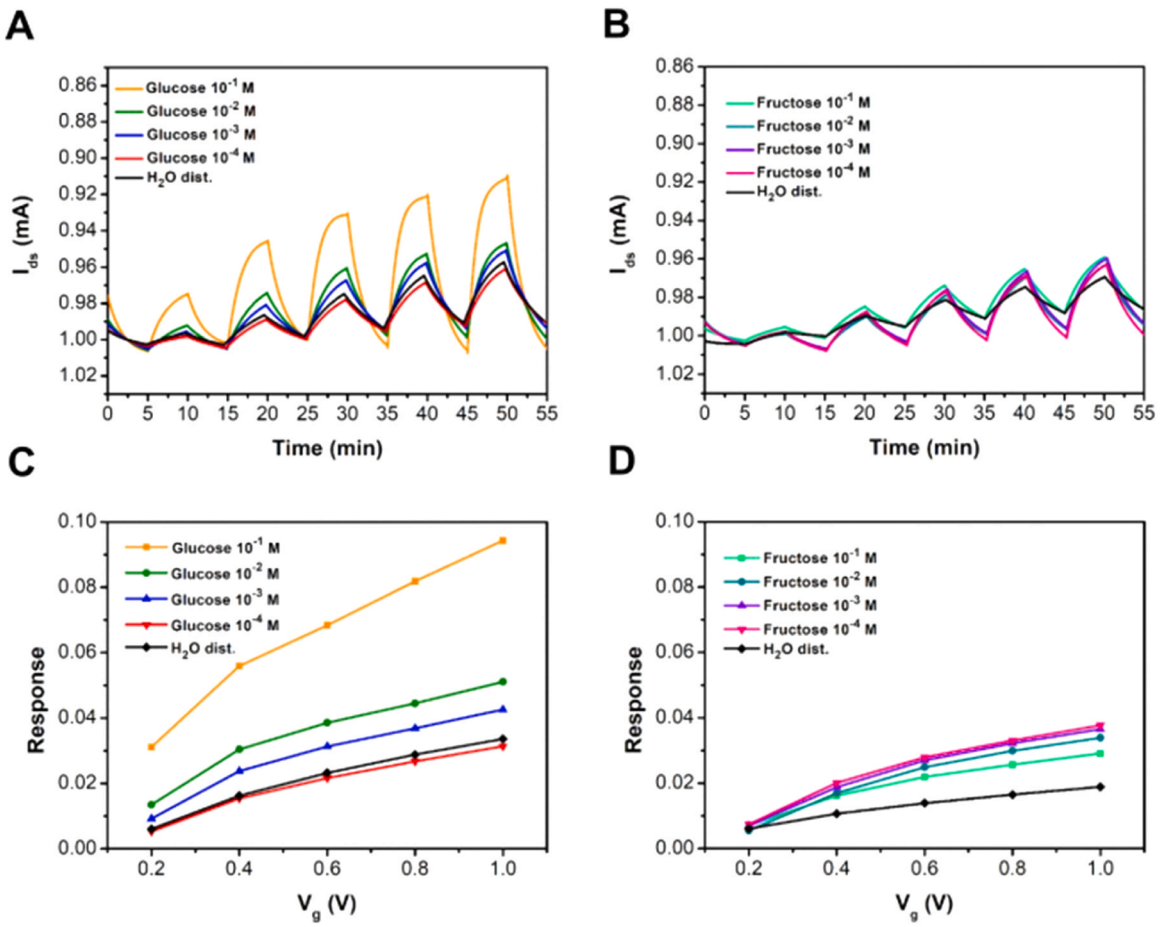

Fig. 4. NanoMIP fiber wire-based sensor properties. A) Drain current (I_{ds}) as a function of time in the presence of different D-glucose concentrations (10^{-6} M, 10^{-5} M, 10^{-4} M, 10^{-3} M, 10^{-2} M and 10^{-1} M) measured pulsing the gate voltage between 0.2 V and 1.0 V. B) Drain current (I_{ds}) as a function of time in the presence of different D-fructose concentrations (10^{-6} M, 10^{-5} M, 10^{-4} M, 10^{-3} M, 10^{-2} M and 10^{-1} M) measured pulsing the gate voltage between 0.2 V and 1.0 V. C) Calculated R of the nanoMIP fiber wire sensor towards different D-glucose concentrations as a function of the applied gate voltage (V_g). D) Calculated R of the nanoMIP fiber wire sensor towards different D-fructose concentrations as a function of the applied gate voltage (V_g).

3.5. Comparison between nanoMIP microwire and nanoMIP fiber wire

The calculated response of the D-glucose nanoMIP microwire sensor to D-glucose and D- fructose as a function of the concentration of the two analytes at the fixed $V_g = 0.8$ V (Fig. 5A) points out that there is a significant difference between the response to D-glucose and D-fructose starting from the 10^{-4} M concentration: at 10^{-6} M and 10^{-5} M concentration, the difference between the response against the two sugars is 0.03 and 0.04 respectively; at 10^{-4} M the difference is 0.08, and at 10^{-1} M the difference is 0.35, confirming that the sensitivity of the device

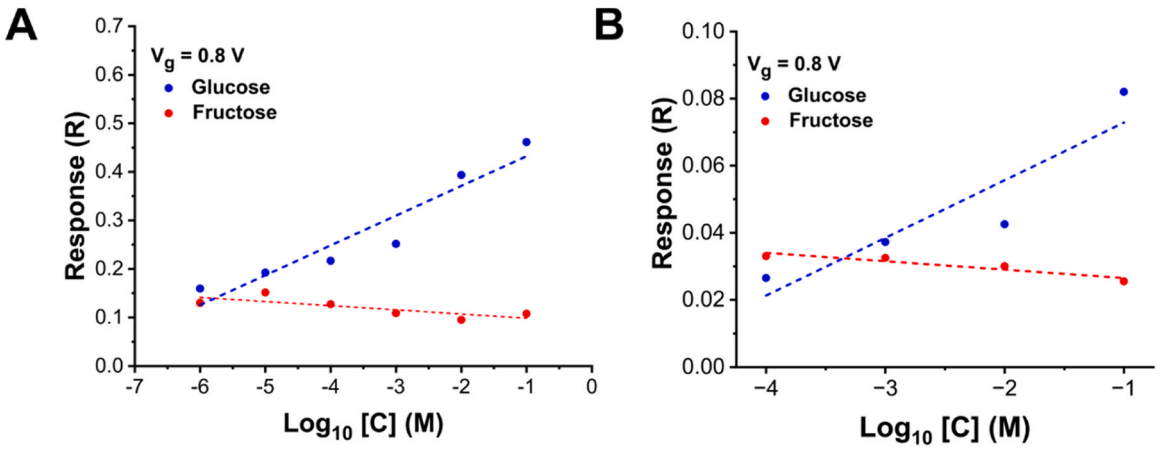

Fig. 5. NanoMIP microwire and nanoMIP fiber wire responses. (A) Calculate response (R) for the microwire sensor towards the logarithm of increasing D-glucose and D-fructose concentrations at $V_g = 0.8$. (B) Calculate response (R) for the nanoMIP fiber wire sensor towards the logarithm of increasing D-glucose and D-fructose concentrations at $V_g = 0.8$.

against the target compound is more evident at higher concentrations. Similarly, the calculated response as a function of different D-glucose and D-fructose concentrations at the fixed $V_g = 0.8$ V for the nanoMIP fiber wire sensor shows a significant difference in the response considering the two analytes (Fig. 5B); the difference in the response has its maximum values at 10^{-2} M concentration (0.015) and 10^{-1} M (0.056). The difference between the response calculated for D-glucose and D-fructose is very small at the lower concentrations of 10^{-4} M and 10^{-3} M, 0.006 and 0.004 respectively.

The limit of detection (LOD), representing the lowest D-glucose concentrations that the device can distinguish from other background signals (in our case, distilled water), is 7.94 * 10^{-8} M for the nanoMIP microwire OECT at V_g 0.8 V, while the LOD for nanoMIP fiber wire is approximately 3 orders of magnitude higher, 2,51 * 10^{-4} M.

The transconductance (g_m) of both the nanoMIP microwire sensor (Fig. 6, blue line) and the non-functionalized microwire sensor (Fig. 6, red line), measured as a function of V_g in the presence of 10^{-1} M D-glucose, appeared to be significantly diverse. In particular, the g_m values related to the nanoMIP wire sensor increase from 0.47 (at 0.2 V) to 0.81 (at 1.0 V), whereas the g_m values related to the non-functionalized microwire sensor vary from 0.05 (at 0.2 V) to 0.16 (at 1.0 V). Transfer characteristics (Fig. 6, black line) and output curves (see SI, Fig. S4) in the V_{ds} range from 0 to −0.6 show behaviors similar of microwire sensor to those of standard OECTs in an electrolytic solution.

Comparing the nanoMIP microwire and the nanoMIP fiber wire sensors (Figs. 4–5), it can be seen that the nanoMIP microwire based sensor has a higher sensitivity for the detection of D-glucose than the nanoMIP fiber wire sensor, as the nanoMIP microwire sensor is able to discriminate D-glucose from D-fructose at a concentration of 10^{-4} M, unlike the nanoMIP fiber wire sensor which shows a significant difference in the response for the two analytes at 10^{-2} M concentration. Furthermore, the nanoMIP fiber wire sensor has a calculated response that is an order of magnitude lower with respect to the nanoMIP microwire sensor, although the trend of the plotted R is the same for both sensors. The lower response to D-fructose confirms the intrinsic selectivity of the nanoMIP-OECT devices to discriminate the target analyte from other interfering compounds.

Regarding the molecular reasons that allow the discrimination between the two monosaccharides, D-glucose and D-fructose are structural isomers that share the same chemical formula but different stereochemical configuration, in particular the arrangement of the hydroxylic groups bound to the ring carbons. D-glucose is a hexose sugar mainly present in a closed conformation with a pyranose ring, whereas D-fructose forms a furanose ring with 5 carbons. Since D-fructose has fewer carbons in the main ring, the overall size of the ring is smaller compared to D-glucose thus reducing and modifying the contact surface with the nanoMIPs and the possibility to interact with them.

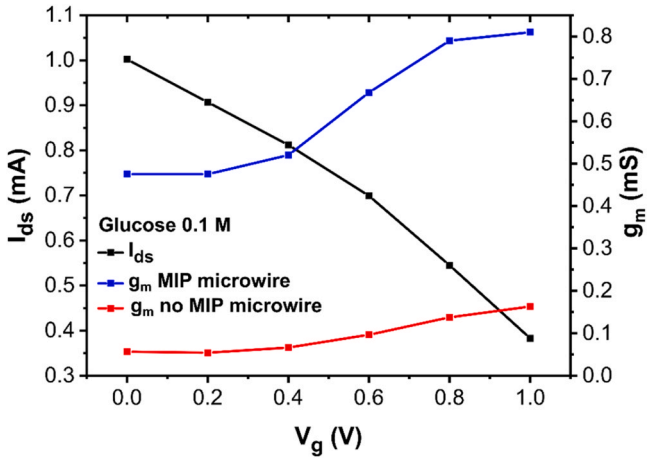

Fig. 6. Transconductance (g_m) of microwire sensor in the presence (blue line) and absence (red line) of nanoMIP functionalization, and transfer curve showing channel current I_{ds} (black line) as a function of increasing gate voltages (from 0 to 1 V) in the presence of 0.1 M D-glucose for nanoMIP microwire.

3.6. *Application of nanoMIP fiber wire OECT in tomato plant monitoring for D-glucose detection*

MIP nanoparticles sensors made with fiber wire geometry were successfully implemented in open field in tomato plants for *in vivo* D-glucose detection, in combination with a non-specific *in vivo* OECT biosensor. The device enabled the continuous *in vivo* monitoring of tomato plants for two months continuously. The fiber wire device with MIP nanoparticle was preferred to microwire geometry for reasons of stability and robustness, since the fiber has to be inserted into the stem of the tomato plant and must have a structure capable of resisting the pressure exerted by the movement of the stem, maintaining elasticity and flexibility.

The normalized D-glucose sensor response (gNR) was plotted alongside the conventional bioristor sensor response to illustrate the temporal trend of D-glucose accumulation. Throughout the experiment, an inverse trend was observed between the sensor response of the non-specific bioristor (R, red curve) and the D-glucose nanoMIP fiber wire sensor (gNR, green curve). Specifically, when the non-specific bioristor (R, red curve) exhibited the expected negative slope, as previously reported [24], the D-glucose nanoMIP sensor displayed an increased gNR from July 14 to August 8, 2022 (Fig. 7). Both sensors demonstrated an overall decrease in their responses, though the decline was slower in the D-glucose nanoMIP fiber, likely due to the accumulation of osmoregulatory molecules. Under drought conditions, the accumulation of soluble sugars— such as glucose, sucrose, fructose, and maltose [59–61] —plays a crucial role in promoting osmotic regulation in plant cells. This phenomenon is consistent with previous reports of drought-stressed soybean leaves, where enhanced sucrose cycling increased the conversion of sucrose to glucose and fructose, improving osmotic regulation under drought conditions. These results not only validate the efficacy of the molecularly imprinted polymer (MIP) approach in selectively detecting specific molecules in plant sap, but they also highlight the sensor potential to further elucidate the defense mechanisms activated by plants during drought stress [62].

4. Conclusions

We demonstrated that the functionalization of an OECT channel with PEDOT:PSS and molecular imprinted polymer nanoparticles can be relevant to fabricating a device sensitive and selective to D-glucose. The presence of MIP nanoparticles has been shown to increase the specific sensitivity to glucose, allowing a selective detection with respect to fructose and realizing a sensor based on reversible processes and suitable for continuous monitoring of composite solutions. To prepare a nanoMIP selective for D-glucose, an acrylamide monomer bearing a phenylboronic acid functionality was chosen for the synthesis, so to favor interactions with cis-diols. As a result, the D-glucose nanoMIPs had an affinity for D-glucose of 1.26 10^4 M^{-1} one order of magnitude higher than that for fructose. In general, the nanoMIP materials display superior characteristics in terms of binding respect other MIPs (bulk and thin films) proposed for sensing glucose, for their homogeneity and fast diffusion kinetics. Integrated into the OECTs, we tested two different channel geometries, one based on full conductive polymer microfiber, and another made by functionalizing a textile fiber on the surface. Both could detect different concentrations of D-glucose in the physiological ranges of biofluids and to discriminate between the main target and other interfering molecules.

The nanoMIP-based OECT sensors showed respectively a LOD of 7.94 * 10^{-8} M for the microwire and a LOD of 2,51 * 10^{-4} M for the fiber wire. As a comparison, among the MIP-based sensors reported for glucose and where the MIP is in the form of layers, a screen printed gold

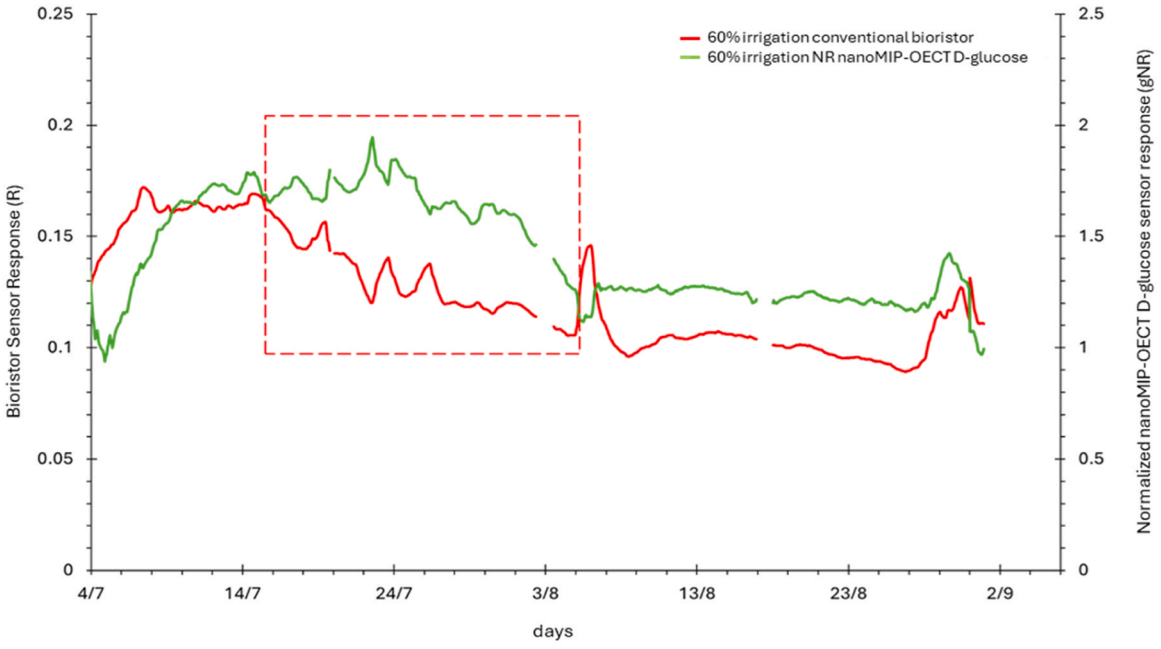

Fig. 7. nanoMIP fiber wire sensor for D-glucose detection and standard bioristor data analysis. R, Bioristor sensor response (60 % irrigation, blue line 60 % irrigation, red line), NanoMIP fiber wire response (Normalized nanoMIP fiber wire for D-glucose response gNR, 60 % irrigation, green line). Red dashed rectangle indicates the drought period.

electrode (Au-SPE) was prepared by electropolymerizing acrylamide/bisacrylamide in the presence of glucose showing a working range from 0.5 to 50 μg/mL (50 $*10^{-6}$ M) and a LOD of 3.32 * 10^{-6} M [63]. Higher sensitivity were reported and a LOD of 30 ppb (3 $*10^{-8}$ M) for interdigitated electrodes and electrochemical transduction with 5 order of linear response [64], demonstrating the nanoMIP OECT microwire sensor is indeed competitive.

In addition, the efficacy of the developed sensor was demonstrated, *in vivo*, as real-time monitoring of tomato plants cultivated in open field, revealing the accumulation of D-glucose under stress in real-time and during the entire length of the plant growth.

CRediT authorship contribution statement

Palermo Nadia: Investigation, Data curation. **Marinangeli Alice:** Investigation, Data curation. **Bossi Alessandra Maria:** Writing – review & editing, Supervision, Methodology, Investigation. **Debbi Gabriele:** Investigation, Data curation. **Bettelli Manuele:** Software, Methodology, Investigation, Data curation. **Dembech Elena:** Writing – review & editing, Writing – original draft, Validation. **Manfredi Riccardo:** Investigation, Data curation. **Coppede Nicola:** Supervision, Methodology, Conceptualization. **Vurro Filippo:** Visualization, Investigation, Data curation. **Martini Vittoria:** Investigation, Data curation. **Janni Michela:** Writing – review & editing, Supervision, Investigation, Data curation.

Declaration of Competing Interest

The authors declare that they have no known competing financial interests or personal relationships that could have appeared to influence the work reported in this paper.

Acknowledgements

AMB thanks the Centro Piattaforme Tecnologiche (CPT) of the University of Verona for the use of the facilities ITC and DLS. The SEM images were kindly performed by Prof. Devid Maniglio using the equipment of the Biotech Lab of the Department of Industrial Engineering of Trento University. AMB and AM thank the Italian Ministry of Research and University doctoral program DM351. AMB states that this work was performed in part under the research program "Dipartimento di Eccellenza 2023–2027" awarded to Dipartimento di Biotecnologie of the Università di Verona. This work was supported in part by the E-Crops Technologies for Digital and Sustainable Agriculture Project funded by the Italian Ministry of University and Research (MUR) through the Programma Operativo Nazionale (PON) Agrifood Program under Contract ARS01_01136. Thanks are due the Made in Italy - Circular and Sustainable (MICS) Extended Partnership funded by the European Union Next-Generation EU (Piano Nazionale di Ripresa e Resilienza (PNRR) - Missione 4, Componente 2, Investimento 1.3 – D.D. 1551.11–10–2022, PE00000004) for financial support.

Appendix A. Supporting information

Supplementary data associated with this article can be found in the online version at doi:10.1016/j.snb.2025.137640.

Data Availability

Data will be made available on request.

References

[1] A. Nawaz, Q. Liu, W.L. Leong, K.E. Fairfull-Smith, P. Sonar, Organic electrochemical transistors for in vivo bioelectronics, Adv. Mater. 33 (2021) 2101874.
[2] T. Nguyen-Dang, et al., Efficient fabrication of organic electrochemical transistors via wet chemical processing, ACS Appl. Mater. Interfaces 14 (2022) 12469–12478.
[3] M. Ghittorelli, et al., High-sensitivity ion detection at low voltages with current-driven organic electrochemical transistors, Nat. Commun. 9 (2018) 1441.
[4] D. Khodagholy, et al., High transconductance organic electrochemical transistors, Nat. Commun. 4 (2013) 2133.
[5] A. Koklu, et al., Microfluidics integrated n-type organic electrochemical transistor for metabolite sensing, Sens. Actuators B Chem. 329 (2021) 129251.
[6] V.F. Curto, et al., Organic transistor platform with integrated microfluidics for in-line multi-parametric in vitro cell monitoring, Microsyst. Nanoeng. 3 (2017) 17028.
[7] C. Yang, et al., Low-power/high-gain flexible complementary circuits based on printed organic electrochemical transistors, Adv. Electron. Mater. 8 (2022) 2100907.

[8] A. Romeo, et al., Drug-induced cellular death dynamics monitored by a highly sensitive organic electrochemical system, Biosens. Bioelectron. 68 (2015) 791–797.
[9] F. Gentile, et al., A biomimetic, biocompatible OECT sensor for the real-time measurement of concentration and saturation of ions in plant sap, Adv. Electron. Mater. 8 (2022) 2200092.
[10] A. Cavallo, et al., Biocompatible organic electrochemical transistor on polymeric scaffold for wound healing monitoring, Flex. Print. Electron 7 (2022) 035009.
[11] J. Ma, et al., Fatigue assessment of construction equipment operators using a sweat lactate biosensor, Int. J. Ind. Erg. 96 (2023) 103472.
[12] I. Gualandi, et al., Textile organic electrochemical transistors as a platform for wearable biosensors, Sci. Rep. 6 (2016) 33637.
[13] M. Berto, et al., Label free urea biosensor based on organic electrochemical transistors, Flex. Print. Electron 3 (2018) 024001.
[14] N. Coppedè, et al., Ion selective textile organic electrochemical transistor for wearable sweat monitoring, Org. Electron 78 (2020) 105579.
[15] G. Tarabella, et al., A single cotton fiber organic electrochemical transistor for liquid electrolyte saline sensing, J. Mater. Chem. 22 (2012) 23830.
[16] M.L. Coluccio, et al., Tailoring chemometric models on blood-derived cultures secretome to assess personalized cancer risk score, Cancers 12 (2020) 1362.
[17] G. Méhes, et al., Organic microbial electrochemical transistor monitoring extracellular electron transfer, Adv. Sci. 7 (2020) 2000641.
[18] K. Butina, F. Filipović, A. Richter-Dahlfors, O. Parlak, An organic electrochemical transistor to monitor *Salmonella* Growth in real-time, Adv. Mater. Interfaces 8 (2021) 2100961.
[19] E. Frantz, J. Huang, D. Han, A.J. Steckl, The effect of nutrient broth media on PEDOT:PSS gated OECTs for whole-cell bacteria detection, Biosens. Bioelectron. X 12 (2022) 100268.
[20] P. Vizzini, et al., Detection of Listeria monocytogenes in foods with a textile organic electrochemical transistor biosensor, Appl. Microbiol. Biotechnol. 107 (2023) 3789–3800.
[21] N. Coppedè, et al., An in vivo biosensing, biomimetic electrochemical transistor with applications in plant science and precision farming, Sci. Rep. 7 (2017) 16195.
[22] M. Janni, et al., *In Vivo* phenotyping for the early detection of drought stress in tomato, Plant Phenom. 2019 (2019) (2019) 6168209.
[23] J. Michela, et al., Real-time monitoring of Arundo donax response to saline stress through the application of in vivo sensing technology, Sci. Rep. 11 (2021) 18598.
[24] F. Vurro, et al., In vivo sensing to monitor tomato plants in field conditions and optimize crop water management, Precis. Agric. 24 (2023) 2479–2499.
[25] D. Amato, et al., Towards in vivo monitoring of ions accumulation in trees: response of an in planta organic electrochemical transistor based sensor to water flux density, light and vapor pressure deficit variation, Appl. Sci. 11 (2021) 4729.
[26] F. Vurro, et al., Development of an in vivo sensor to monitor the effects of vapour pressure deficit (VPD) changes to improve water productivity in agriculture, Sensors 19 (2019) 4667.
[27] H. Liu, et al., Ultrafast, sensitive, and portable detection of COVID-19 IgG using flexible organic electrochemical transistors, Sci. Adv. 7 (2021) eabg8387.
[28] D. Gentili, et al., Integration of organic electrochemical transistors and immuno-affinity membranes for label-free detection of interleukin-6 in the physiological concentration range through antibody–antigen recognition, J. Mater. Chem. B 6 (2018) 5400–5406.
[29] V. Preziosi, et al., Immuno-sensing at ultra-low concentration of TG2 protein by organic electrochemical transistors, Biosensors 13 (2023) 448.
[30] C. Liao, C. Mak, M. Zhang, H.L.W. Chan, F. Yan, Flexible organic electrochemical transistors for highly selective enzyme biosensors and used for saliva testing, Adv. Mater. 27 (2015) 676–681.
[31] N. Saraf, E.R. Woods, M. Peppler, S. Seal, Highly selective aptamer based organic electrochemical biosensor with pico-level detection, Biosens. Bioelectron. 117 (2018) 40–46.
[32] C. Peruzzi, et al., Interfacing aptamers, nanoparticles and graphene in a hierarchical structure for highly selective detection of biomolecules in OECT devices, Sci. Rep. 11 (2021) 9380.
[33] O. Norrlöw, M. Glad, K. Mosbach, Acrylic polymer preparations containing recognition sites obtained by imprinting with substrates, J. Chromatogr. A 299 (1984) 29–41.
[34] S. Yang, Y. Wang, Y. Jiang, S. Li, W. Liu, Molecularly imprinted polymers for the identification and separation of chiral drugs and biomolecules, Polymers 8 (2016) 216.
[35] A. Lamaoui, J.J. García-Guzmán, A. Amine, J.M. Palacios-Santander, L. Cubillana-Aguilera, Synthesis techniques of molecularly imprinted polymer composites. Molecularly Imprinted Polymer Composites, Elsevier, 2021, pp. 49–91, https://doi.org/10.1016/B978-0-12-819952-7.00002-0.
[36] Y. Hoshino, T. Kodama, Y. Okahata, K.J. Shea, Peptide imprinted polymer nanoparticles: a plastic antibody, J. Am. Chem. Soc. 130 (2008) 15242–15243.
[37] L. Cenci, et al., Synthesis and characterization of peptide-imprinted nanogels of controllable size and affinity, Eur. Polym. J. 109 (2018) 453–459.
[38] F. Canfarotta, A. Poma, A. Guerreiro, S. Piletsky, Solid-phase synthesis of molecularly imprinted nanoparticles, Nat. Protoc. 11 (2016) 443–455.
[39] A.R. Guerreiro, I. Chianella, E. Piletska, M.J. Whitcombe, S.A. Piletsky, Selection of imprinted nanoparticles by affinity chromatography, Biosens. Bioelectron. 24 (2009) 2740–2743.
[40] A. Chiappini, L. Pasquardini, A.M. Bossi, Molecular imprinted polymers coupled to photonic structures in biosensors: the state of art, Sensors 20 (2020) 5069.
[41] A. Marinangeli, I. Chianella, E. Radicchi, D. Maniglio, A.M. Bossi, Molecularly imprinted polymers electrochemical sensing: the effect of inhomogeneous binding sites on the measurements. a comparison between imprinted polyaniline versus nanoMIP-doped polyaniline electrodes for the EIS detection of 17β-estradiol, ACS Sens 9 (2024) 4963–4973.
[42] L. Bai, et al., Biological applications of organic electrochemical transistors: electrochemical biosensors and electrophysiology recording, Front. Chem. 7 (2019) 313.
[43] O. Parlak, S.T. Keene, A. Marais, V.F. Curto, A. Salleo, Molecularly selective nanoporous membrane-based wearable organic electrochemical device for noninvasive cortisol sensing, Sci. Adv. 4 (2018) eaar2904.
[44] P.S. Sharma, A. Garcia-Cruz, M. Cieplak, K.R. Noworyta, W. Kutner, 'Gate effect' in molecularly imprinted polymers: the current state of understanding, Curr. Opin. Electrochem 16 (2019) 50–56.
[45] L. Zhang, et al., Chirality detection of amino acid enantiomers by organic electrochemical transistor, Biosens. Bioelectron. 105 (2018) 121–128.
[46] L. Zhang, et al., Selective recognition of Histidine enantiomers using novel molecularly imprinted organic transistor sensor, Org. Electron 61 (2018) 254–260.
[47] L. Zhang, et al., Highly selective and sensitive sensor based on an organic electrochemical transistor for the detection of ascorbic acid, Biosens. Bioelectron. 100 (2018) 235–241.
[48] A.B. Woeppel, J. Schaefer, H.J. Kim, B.W. Boudouris, S.P. Beaudoin, Ion-selective organic electrochemical transistor sensors using molecularly imprinted polymers, ACS Appl. Polym. Mater. 4 (2022) 6667–6674.
[49] P. Hao, et al., Dual-analyte sensing with a molecularly imprinted polymer based on enhancement-mode organic electrochemical transistors, ACS Appl. Mater. Interfaces 15 (2023) 30567–30579.
[50] K. Tang, et al., Organic electrochemical transistor with molecularly imprinted polymer-modified gate for the real-time selective detection of dopamine, ACS Appl. Polym. Mater. 4 (2022) 2337–2345.
[51] H. Bernheimer, W. Birkmayer, O. Hornykiewicz, K. Jellinger, F. Seitelberger, Brain dopamine and the syndromes of Parkinson and Huntington Clinical, morphological and neurochemical correlations, J. Neurol. Sci. 20 (1973) 415–455.
[52] J.M. Swanson, et al., Dopamine genes and ADHD, Neurosci. Biobehav. Rev. 24 (2000) 21–25.
[53] H. Kaur, M. Manna, T. Thakur, V. Gautam, P. Salvi, Imperative role of sugar signaling and transport during drought stress responses in plants, Physiol. Plant 171 (2021) 833–848.
[54] M. Manna, et al., Transcription factors as key molecular target to strengthen the drought stress tolerance in plants, Physiol. Plant 172 (2021) 847–868.
[55] P.V.V. Prasad, S.R. Pisipati, I. Momčilović, Z. Ristic, Independent and combined effects of high temperature and drought stress during grain filling on plant yield and chloroplast ef-tu expression in spring wheat: effects of temperature and drought on wheat plants, J. Agron. Crop Sci. 197 (2011) 430–441.
[56] F. Tardieu, T. Simonneau, B. Muller, The physiological basis of drought tolerance in crop plants: a scenario-dependent probabilistic approach, Annu. Rev. Plant Biol. 69 (2018) 733–759.
[57] Á. Camisón, M. Ángela Martín, F.J. Dorado, G. Moreno, A. Solla, Changes in carbohydrates induced by drought and waterlogging in Castanea sativa, Trees 34 (2020) 579–591.
[58] P.-X. Sun, et al., Determination of glucose by a molecular capacitor array based using a 3-(Acrylamido) phenylboronic acid prepared molecularly imprinted polyacrylamide cryogel, Anal. Lett. 54 (2021) 2789–2800.
[59] F. Secchi, M.A. Zwieniecki, Accumulation of sugars in the xylem apoplast observed under water stress conditions is controlled by xylem pH, Plant Cell Environ. 39 (2016) 2350–2360.
[60] Q. Liu, C. Wu, L. Gao, L. Ying, Coordination between non-structure carbohydrates and hydraulic function under different drought duration, intensity, and post-drought recovery, Environ. Exp. Bot. 215 (2023) 105485.
[61] V. Buffagni, et al., Shaping durum wheat for the future: gene expression analyses and metabolites profiling support the contribution of BCAT genes to drought stress response, Front. Plant Sci. 11 (2020) 891.
[62] Y. Du, et al., Effect of drought stress on sugar metabolism in leaves and roots of soybean seedlings, Plant Physiol. Biochem 146 (2020) 1–12.
[63] A. Diouf, B. Bouchikhi, N. El Bari, A nonenzymatic electrochemical glucose sensor based on molecularly imprinted polymer and its application in measuring saliva glucose, Mater. Sci. Eng. C. 98 (2019) 1196–1209.
[64] N. Asghar, et al., Real-time and online monitoring of glucose contents by using molecular imprinted polymer-based IDEs sensor, Appl. Biochem. Biotechnol. 189 (2019) 1156–1166.

Dr. Filippo Vurro is a post-doctoral researcher at IMEM-CNR Parma. He holds a bachelor's degree in Biology, a master's degree in Chemistry, and a PhD in Materials Science from the University of Parma. With a multidisciplinary background, Dr. Vurro's research primarily involves developing and preparing in-vivo electrochemical biosensors for plants. He applies multivariate statistical methods and machine learning techniques to analyze and interpret complex data. His expertise also extends to Metabolomics, using NMR spectroscopy in both biomedical and agronomic applications. In May 2019, in the framework of the Fascination of Plants Day 2019 in Matera, he won the first prize in the Smart Plants contest. In December 2019, during the Nanoday19 in Milano, he received the recognition as best presentation in the life science session. He has authored 25 scientific publications (H-index of 10).

Dr. Elena Dembech is a Post Doctoral researcher at the CNR Institute of Materials for Electronics and Magnetism (IMEM-CNR). She holds a Master's degree in Molecular Biology (University of Parma, Italy) and a PhD in Life Sciences and Biotechnology (University of Parma, Italy), with a strong background in the branch of biochemistry dedicated to the study of genes and proteins from a phylogenetic, structural and functional point of view.

Dr. Dembech is deeply fascinated by the possibility of applying the study of biological macromolecules, which underpin the evolution and survival of living species, to practical needs in the medical field and beyond. She is currently working on the development and application of OECTs for the detection of target molecules using biological elements such as enzymes, aptamers, antibodies and MIPs.

Dr. Riccardo Manfredi is graduated in Chemistry at the University of Parma in 2018 and continued his studies as a PhD student in Materials Science and Technology at the CNR-IMEM Institute in Parma, obtaining the title in May 2022. From October 2022 to December 2023 he was a researcher and KLOPMANN employee at the CNR-NANOTEC Institute in Lecce. Since April 2024, he has been a fixed-term researcher at the CNR-SCITEC "Giulio Natta" Institute in Genoa. Dr.Manfredi's research path has been focused on the development of polymer-small molecule blends to obtain stable, sensitive and selective electrochemical biosensors for the field of precision agriculture during his PhD, and then on the development of ink-jet printed OLEDs during the CNR-NANOTEC period. His current research at CNR-SCITEC aims to develop and characterize flexible lead-free polymer-based composites with piezoelectric properties for energy harvesting through different film formation techniques.

Gabriele Debbi earned his master degree in Industrial Chemistry from the University of Parma in 2020. He has worked as research fellow on conductive polymers and molecular cavitands. His research interests are high-property materials and special-application polymers.

Dr. Manuele Bettelli is a researcher with solid experience in X-ray and gamma detector technology, specializing in the use of CdZnTe crystals. He currently works as a Level III Technologist at the Institute of Materials for Electronics and Magnetism (IMEM) of the C.N.R., where he serves as the scientific director for projects related to the engineering, development, and characterization of gamma detectors, as well as the installation of bioristor sensors in crop fields. Dr. Bettelli holds a PhD in "Materials Science and Technology" from the University of Parma, where he also completed a Master's Degree in Physics with a grade of 110/110. His technical expertise includes photolithography, the design of readout electronics for in-vivo sensors, and the development of simulation software for detectors. He is a founding member of the startup "Plantbit s.r.l.," a CNR spin-off specializing in in-vivo plant monitoring sensors, and has authored 72 scientific articles, two international patents, and has an H-index of 15 on Scopus. His honors include several grants and awards for young researchers. Dr. Bettelli collaborates with numerous academic and industrial institutions.

Alice Marinangeli is a PhD student in Biotechnology at University of Verona, and she is passionate about the development of sensors and their application in biomedical, industrial and environmental fields. Her expertise includes the synthesis and characterization of biomimetic polymers in a nanometric format by molecular imprinting technique. She is dedicated to use these polymers as synthetic receptor to design optical and electrochemical sensors.

Prof. Alessandra Maria Bossi, Prof. in Analytical Chemistry, holds the Chair of Analytical Chemistry at the University of Verona (Italy). She has a MSc in Biochemistry (State University of Milano, Italy) and a PhD in Polymer Chemistry (Cranfield University, UK). AM Bossi founded and currently leads the Molecular Imprinting and Analytical Sciences Group at the Dept. of Biotechnology, University of Verona. Her research is dynamic and concentrated on advancing the field of molecularly imprinted polymers (MIPs), where she has consistently pioneered innovations in both the synthesis and application of MIPs. AM Bossi's is funded by both public and private institutions, including the Italian Ministry of University and the European Union. She is regularly invited to international conferences and is author of more than 110 papers on peer review international journals and of 7 patents.

Dr. Nadia Palermo is a Postdoctoral researcher at the Institute of Materials for Electronics and Magnetism (IMEM-CNR). She completed her degree in Biology and Biomedical Applications at the University of Parma, Italy, where she also earned her PhD in Biotechnology and Biosciences. During her doctoral studies, she focused on wheat phenotyping under heat stress, examining its morphological, molecular, and biochemical characteristics. Currently, her research centers on the use of in vivo biosensors to study plants under both abiotic stress and normal conditions, with the goal of minimizing water usage. Additionally, she conducts phenotyping analyses on plants treated with carbon dots.

Dr. Vittoria Martini completed her Master of Science in Industrial Chemistry at the University of Parma, Italy, in 2021, where she focused on the study of host-guest supramolecular complexes derived from cucurbit[8]uril and heterocyclic guests. Following her graduation, she undertook an 8-month research fellowship at the CNR-IMEM institute in Parma, where she worked on the development of biosensors for plants, utilizing organic electrochemical transistors and molecularly imprinted polymers (MIPs) technology. Currently, Vittoria is in the final stages of her PhD in Chemical Sciences at the University of Parma, where she is developing novel catalytic approaches for the synthesis of value-added compounds. Her doctoral research initially focused on the Catellani reaction for the synthesis of biaryl derivatives. During the second year of her PhD, she spent six months as a visiting researcher in the group of Prof. Geraldine Masson at CNRS-ICSN in Paris, where she worked on asymmetric synthesis and organocatalysis. In the same year, she also spent six months in the Exploratory Chemistry Unit at Chiesi, contributing to Preclinical Chemistry Research & Drug Design. In the final year, she has been exploring photocatalysis for the synthesis of unnatural amino alcohols.

Dr. Michela Janni is permanent researcher in CNR at the Institute of Materials for Electronics and Magnetism (IMEM-CNR) since 2011.She has a master degree in Agriculture Science and Technology at University of Tuscia and a PhD in Vegetal Biotechnology. Here work focused on plant genetics and physiology in frame of the ongoing climate change, in the exploitation of plant phenotyping as strategy to select more adaptable genotypes for breeding. In the last 8 years, the research activity focused on development and application of *in vivo* biosensors to improve water use efficiency in agriculture and to understand the mechanisms exploited by plants to overcome abiotic resistance. She is co-funder of the startup PlantBit. She is leading the Expert working group for plant phenotyping in the wheat initiative.

Dr. Nicola Coppedè is a researcher at IMEM-CNR. He graduated in Physics at the University of Pisa in 2001 and has a PhD in Physics at the University of Trento in 2006. His main activities are the development of biosensors for organic bioelectronics, focused also on IOT applications. He developed biosensors based on organic electrochemical transistors on textile fabric foe sweat monitoring, integrated pressure sensors in polymers and composites, biocompatible electrochemical sensors for in vivo plant monitoring. He develops innovative sensors from organic materials, nanostructured oxides and hybrid materials. In the past he was a researcher at the Magna Graecia University of Catanzaro in sensors in the biomedical field. He is the author of over 90 scientific publications in international journals, author of 9 patents, h-index: 26. In 2009 he was a teacher of the MEMS Master's course at the University of Trento.